

Chaos in Nonlinear Dynamical Systems – Helicopter Flight-data Analysis

James H. Taylor¹ and S. Salamat Sharif²

Department of Electrical and Computer Engineering

University of New Brunswick

Fredericton, N. B., CANADA, E3B 5A3

E-mail: 1) jtaylor@unb.ca, 2) salamat@ee.unb.ca

; *Abstract* – The nonlinear dynamic behaviour of a modern, multi-purpose helicopter is considered in this article. The main objective of this study is to characterize the helicopter’s vibration mechanism(s) – i.e., to determine if the vibrations are periodic or chaotic. This study involved analyses of flight data, specifically records of acceleration for two different airspeeds with a sampling rate of 1024 Hz.

Some background in the theory of chaos in nonlinear dynamical systems is discussed, and approaches for the identification of chaos in time series data are presented. Several topics including delay-coordinate embedding theory, delay time and dimension determination, and maximal Lyapunov exponent computation for chaotic systems are described. In each section, helicopter flight data sets are examined and analyzed, and the results are compared with those for classical chaotic systems. Results for classical problems adds tutorial value as well as confirming our helicopter studies. Finally, implications regarding the possibility of chaotic behaviour in the flight data are discussed.

1 Introduction

An understanding of the identification and control of chaotic systems has improved tremendously in the last two decades [1]-[21]. Chaotic behaviour can only occur in systems with nonlinear dynamics. The recognition of chaos in a complex dynamical system is very complicated. An important characteristic of a chaotic system is its sensitive dependence on initial conditions. The trajectories of such systems can be markedly different even for very close initial conditions. This factor makes the predictability of these systems very difficult and even impossible in the long run. It also introduces new and challenging problems in the area of control.

In many cases, the chaotic behaviour of a system may be mistaken for randomness or noise effects. A system with nonlinearity and random inputs or measurement noise can also produce irregular trajectories. However, a random input is not the only possible source of irregular behaviour in a system; nonlinear chaotic systems can have very irregular output with purely deterministic dynamics and inputs. One important issue in such systems is the discrimination of chaos from randomness. This factor also has very important implications for controlling nonlinear systems. If a system

shows some signs of chaotic behaviour, then it may be controlled with some of the methods which are proposed in the literature [6, 8, 10, 13, 14, 15].

Chaos may exist in classical systems (represented by mathematical models) or real-life systems. Examples of classical systems include the logistic, tent and Hénon maps in the realm of discrete systems, and the Lorenz and Rössler differential equations for continuous-time dynamical systems [2]. Some real-life systems in which chaos has been identified are complex chemical reactions, pendula with periodic forcing functions [2], NMR laser data, human breath rate, vibrating spring data, foetal electrocardiogram signals [8], among others.

In most real-life situations, system behaviour is characterized by time series data sequences available from measurement. For this reason, useful methods for analyzing chaotic systems should be able to deal with time series data. These data can be measurements of only one variable, or measurements of several variables. The first step in the analysis of time series data was introduced in *Geometry from a time series* [16], in which state-space reconstruction of time series data was proposed for the first time. The mathematical justification of this approach was presented in [21]. Based on a mathematical proof given in [21], the reconstructed state space is diffeomorphically (one-to-one and invertible) equivalent to the original state space of the real-life system.

In delay-coordinate reconstruction, the selection of time delay and dimension are the most important issues [5, 9, 11, 12, 19]. For the calculation of time lag, different approaches are proposed in the literature [5, 11]. Among them, the autocorrelation function and mutual information approach are the most general and common [15]. Among the different techniques of the calculation of embedding dimension, the “false nearest neighbours” method has attracted the most attention [9].

By appropriate selection of time delay and embedding dimension, the time series data can be reconstructed in the delay-coordinate state space. In this space, the chaotic behaviour of the nonlinear dynamical system can be studied. A common method for the identification of chaos in state-space systems is to calculate the maximal Lyapunov exponent [14]. The calculation of this exponent from time series data has been extensively considered in the literature [7, 17, 18].

The organization of this article is as follows. In Section 2, the delay-coordinate state-space reconstruction of time series data is discussed. In Section 3, the calculation of the optimal time delay for delay-coordinate reconstruction is described and carried out. In Section 4, the dimension calculation of the reconstructed state space is addressed and also executed. In Section 5, the computation of the maximal Lyapunov exponent for time series data and its use in the identification of chaos are considered, and results are presented. In Section 6, concluding remarks about the possible presence of chaos are provided.

2 Time Series and State Space Reconstruction via Delay-Coordinate Embedding

In most cases, observations of a real system are in the form of time series data, not a state-space representation. However, the more effective approaches for studying deterministic dynamical systems involve describing the system in an appropriate state space. For this reason, time series data should be converted into state-space vectors. This procedure is known as *state-space reconstruction*, which is based on a theorem attributed to Takens [21].

2.1 State Space Models

A state space is a finite-dimensional vector space, \mathfrak{R}^m . In this space, a state is denoted by a vector $\mathbf{x} \in \mathfrak{R}^m$. The dynamics of a discrete-time system can be described in state space by an m -dimensional *map*, \mathbf{F} ,

$$\mathbf{x}_{n+1} = \mathbf{F}(\mathbf{x}_n, n), \quad (1)$$

where the index n denotes the discrete time instants; continuous-time systems are governed by a *flow* (a system of m first-order ordinary differential equations),

$$\frac{d}{dt}\mathbf{x}(t) = \mathbf{f}(\mathbf{x}(t), t), \quad t \in \mathfrak{R} \quad (2)$$

If \mathbf{F} does not depend on n , or \mathbf{f} does not depend on t , then the map or flow is called *autonomous* or *time-invariant*; hereafter we will consider only those cases. A sequence of points \mathbf{x}_n solving Equation (1), or continuous solution $\mathbf{x}(t)$ satisfying Equation (2), is called a *trajectory*, and \mathbf{x}_0 (or $\mathbf{x}(0)$) the *initial condition*. The orbit of \mathbf{x} under \mathbf{F} is the set of points $\{\mathbf{x}, \mathbf{F}(\mathbf{x}), \mathbf{F}^2(\mathbf{x}), \dots\}$, and the trajectory of $\mathbf{x}(t)$ under \mathbf{f} is the solution of the indicated ordinary differential equation, usually obtained by numerical integration.

Certain solutions or trajectories are particularly important in characterizing the behaviour of nonlinear dynamic systems; for non-chaotic systems these are *fixed points* and *closed trajectories* (period- K orbits or limit cycles). A fixed point \mathbf{p} satisfies $\mathbf{F}(\mathbf{p}) = \mathbf{p}$ or $\mathbf{f}(\mathbf{p}) = 0$; in other words, if $\mathbf{x}_0 = \mathbf{p}$ in Equation (1), then $\mathbf{x}_n = \mathbf{p}$, $n = 1, 2, \dots$, or, in Equation (2), $\mathbf{x}(t) \equiv \mathbf{p}$, $\forall t > 0$. Informally, a closed trajectory satisfies $\mathbf{x}_{n+K} = \mathbf{x}_n$ for some period K or $\mathbf{x}(t) = \mathbf{x}(t + \tau)$ for some period τ . The period K is the minimum value for which $\mathbf{F}^K(\mathbf{x}) = \mathbf{x}$, and similarly τ is the smallest value for which $\mathbf{x}(t) = \mathbf{x}(t + \tau)$, $\forall t > 0$. A (non-chaotic) *attractor* of a system is a fixed point or closed trajectory such that for a set of near-by initial conditions the resulting solutions will be attracted to it after some transient time or, more commonly, as n or t approaches infinity. Non-chaotic attractors are stable fixed points and stable limit cycles. The set of initial conditions leading to the same attractor is called the attractor's *basin of attraction*. Note that the concept of attractor may also be extended

to systems with chaotic behaviour, but such a concept and definition is not required here.

For many physical systems, a state-space flow model, Equation (2), is not available; rather, observations of the system variables are taken, including measurements of one or several quantities which depends on the current state of the system. Given a scalar signal, $s(t)$, regularly sampled at time interval τ_s starting at some time t_0 , the n th sample can be represented as:

$$s_n = s(t_0 + (n - 1)\tau_s) + \eta_n, \quad n = 1, 2, \dots, \quad (3)$$

where η_n is the measurement noise. A delay-coordinate reconstruction can be formed by plotting the time series versus one or more time-delayed version(s) of it. For a 2-dimensional reconstruction, we plot the delay vector $\mathbf{y}(n) = [s_n, s_{n-V}]$, $n = V + 1, V + 2, \dots$, where V is the *lag* or *sampling delay*, i.e., the difference between the adjacent components of the delay vector in number of samples. For a d -dimensional reconstruction, the delay vector, $\mathbf{y}(n)$ can be written as:

$$\mathbf{y}(n) = [s_n, s_{n-V}, \dots, s_{n-(d-2)V}, s_{n-(d-1)V}], \quad n = (d - 1)V + 1, \dots \quad (4)$$

One of the major issues in the embedding approach is: Under what conditions is the trajectory of the reconstructed state space equivalent to the original unknown trajectory \mathbf{x}_n or $\mathbf{x}(t)$? It was proved by Takens [21] that if the dimension of the delay-coordinate space, d , is sufficiently large, the attractor formed by the $\mathbf{y}(n)$ vector is equivalent to the attractor in the original space. Specifically, if the dimension of the reconstructed space, d , is larger than twice the *box counting dimension* m of the attractor (or the number of *active* degrees of freedom), the equivalence of the spaces is guaranteed. In some applications, a smaller value of d can also be sufficient [1]. Based on these results, if the dimension of the original attractor is not very high, the reconstruction is possible even if the dimension of the original system is very high. Systems with this characteristic include hydrodynamic flows and lasers [8].

The selection of d , the dimension of the state-space reconstruction, and V , the sampling delay (or $T = V\tau_s$, the time lag), are of great importance, and needs detailed analysis. In many applications, the product $d \cdot V$ is the governing factor for the validity of the delay-coordinate reconstruction [10]. However, the separation of the process of determining d and V makes their calculation easier, albeit perhaps conservative.

The calculation of V and d are discussed in Sections 3 and 4, respectively. From a mathematical point of view, the selection of V has no effect on the embedding of a noise-free time series. However, in practical applications and for data contaminated with noise, a good choice of V has an important impact on the analysis [4]. If V is too small in comparison with the dynamic variation of the system, successive elements of the delay vectors are strongly correlated. If V is too large, successive elements are almost independent. Several approaches are proposed in the literature for the calculation of an optimal value of the sampling lag. Among these methods, the use of the *autocorrelation function* and *mutual information* (see Section 3) are the most

common. Optimal values of V can be verified through the visualization of the data in a two-dimensional embedding space.

2.2 Time Series Data

The dynamical system considered in this article is characterized by helicopter flight data. Two sets of data are examined, each comprised of acceleration signals (calibration withheld) for two different airspeeds (also withheld). The time series data were sampled at $f_s = 1024$ Hz with the nominal rotor speed of $f_n = 3.57$ Hz. The predominant frequency is the blade passing frequency, $f_{BP} = 5f_n = 17.85$ Hz. The data were sampled when the active vibration control system was switched off.

In this study, the two sets of data are referred to as flight data-set one (FDS₁) and flight data-set two (FDS₂). The time evolution of the whole data sets and the first 1000 samples are shown in Figures 1 and 2, respectively.

As a preliminary investigation, the power spectrum of these data was also calculated; the results are presented in Figure 3. As shown in this figure, the highest amplitude pertains to the normalized blade passing frequency, $f_{BP}/1024 = 0.0174$ and lines also occur at higher harmonics; however, we observe that substantial power is also present over a broad range of frequencies. The general sources of broad band frequency content can be random noise or chaos; since the time series plots appear to be quite clean (Figure 2), the presence of chaos in the time series data may be tentatively suspected.

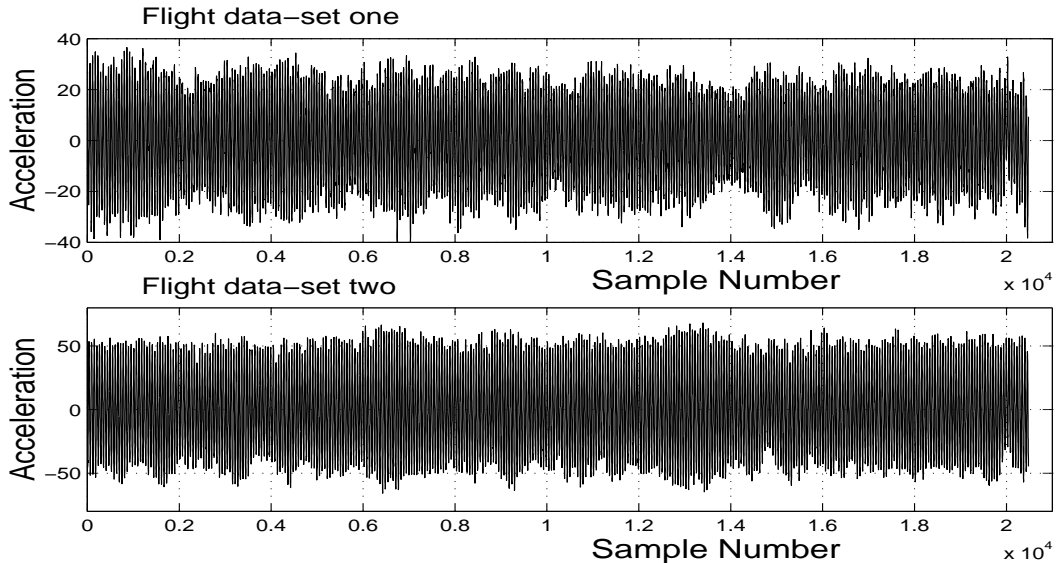


Figure 1: The time evolution of data sets FDS₁ and FDS₂

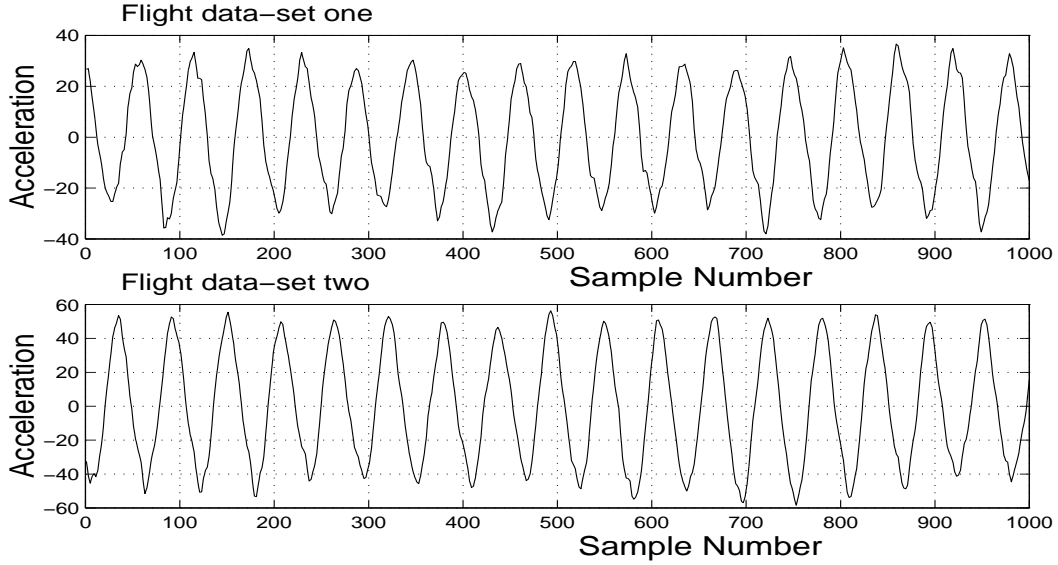


Figure 2: The time evolution of the first 1000 samples of FDS_1 and FDS_2

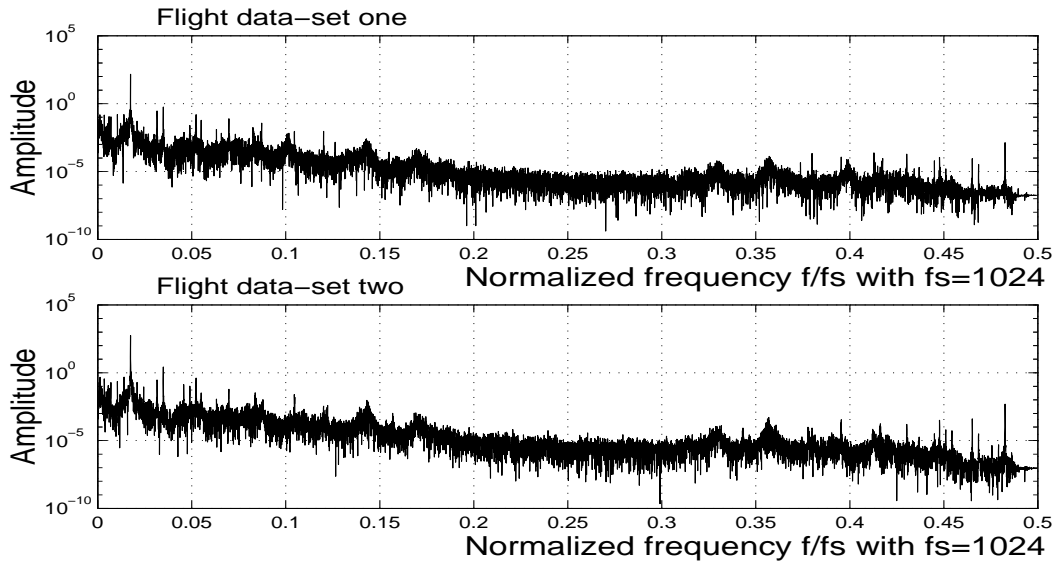


Figure 3: Power spectra of data sets FDS_1 and FDS_2

2.3 Hénon Map and Lorenz System

In order to verify the results obtained for the helicopter flight data, two classical models are also addressed in this study. The Hénon Map and Lorenz System are selected, as examples of a discrete- and continuous-time chaotic system, respectively. The calculated values for these models are compared with the reported values in the literature, and very close conformation have been obtained. This conformation gives us increased confidence about the accuracy of our analysis.

The Hénon Map has states x_n, y_n and is described by

$$\begin{cases} x_{n+1} = 1 - ax_n^2 + y_n \\ y_{n+1} = bx_n, \end{cases} \quad (5)$$

where $a = 1.4$ and $b = 0.3$ lead to chaotic behaviour. The time evolution of the Hénon Map in the 2-dimensional state space is shown in Figure 4.

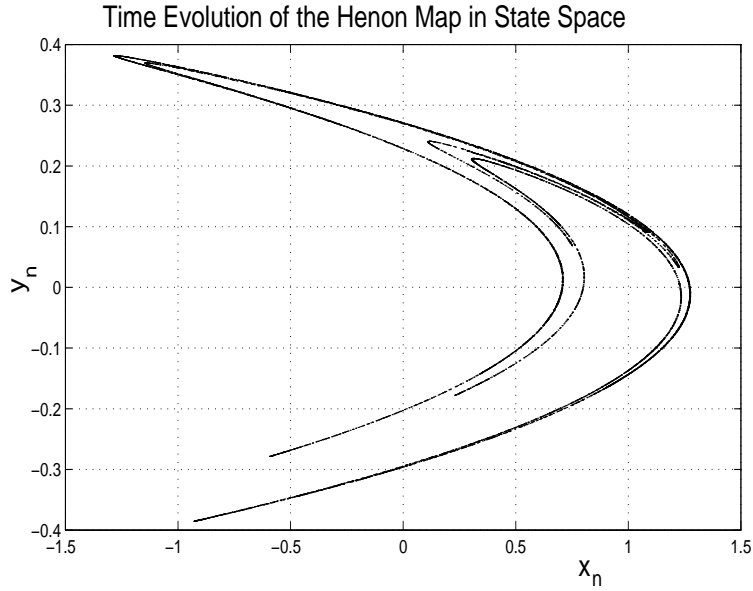


Figure 4: The time evolution of Hénon Map in its state space

The Lorenz System can be formulated as:

$$\begin{cases} \dot{x} = \sigma(y - x) \\ \dot{y} = x(R - z) - y \\ \dot{z} = xy - bz, \end{cases} \quad (6)$$

where $\sigma = 16.0$, $R = 45.92$ and $b = 4.0$ produce chaotic behaviour. The three state variables of this system are two components of temperature and one component of velocity in the convection problem. For comparison of the Lorenz System and the helicopter time series data, the time evolution and power spectrum of the three states of this system are shown in Figures 5 and 6, respectively.

3 Calculation of Optimal Time Delay

From a mathematical point of view, if an infinite amount of infinitely accurate data is available, there is no limit on the choice of sampling delay, except certain multiples

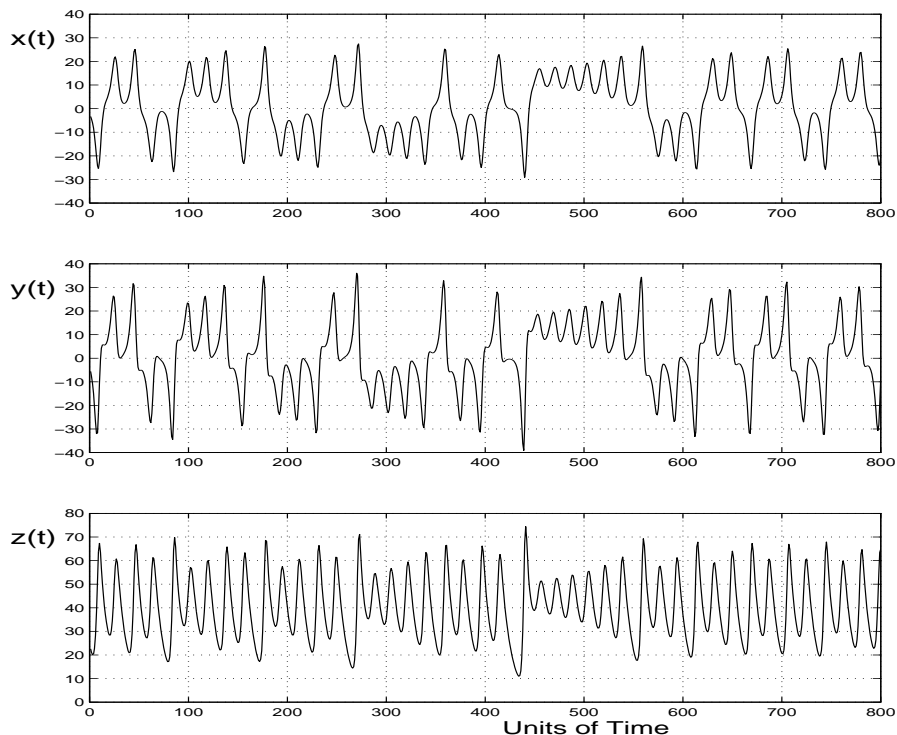


Figure 5: Time evolution of the three states of the Lorenz System

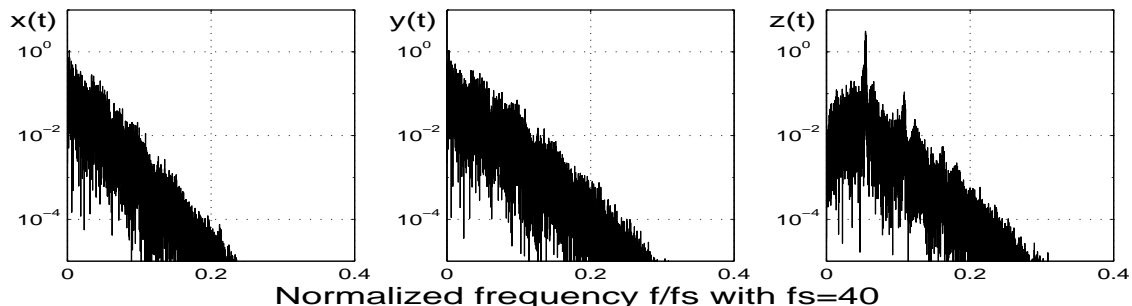


Figure 6: Power spectra of the three states of the Lorenz System

of the precise period of a periodic signal. These conditions cannot be met in real-life data, and an optimal choice of sampling delay plays an important role in the analysis of the reconstructed system. The selection of sampling delay, V , should primarily be based on the following considerations:

1. If the selected sampling delay is too short, the adjacent points (s_n and s_{n-V}) will not be sufficiently independent (will have almost the same information). This condition is also called redundancy [3]. In addition, if the data are noisy, and the variation of the signal during the interval covered by one sample of

vector $\mathbf{y}(n)$, $d \cdot V \cdot \tau_s$ time units, is less than the noise level, the vector will have no information.

2. If the sampling delay selected is too large, any relation between s_n and s_{n-V} can be regarded as randomness due to the sensitive nature of the chaos. This is a central problem with chaotic systems, where the autocorrelation function decays very rapidly.

As a result, an optimal sampling delay should be large enough to give rather independent values for s_n and s_{n-V} , and not too large that it gives completely independent s_n and s_{n-V} . Techniques for the optimal selection of sampling delay have been discussed in the literature extensively. Many of these methods are appropriate only for a specified application. Here, two methods which give satisfactory results in most applications are discussed. These methods deal with the statistical behaviour of the signal, as explained below.

3.1 Time Delay Calculation: Autocorrelation Method

In this approach, the autocorrelation function of the signal is used to identify the optimal value of sampling delay. The autocorrelation function for each sampling delay V can be defined as follows:

$$C_T = \frac{\langle (s_n - \langle s \rangle)(s_{n-V} - \langle s \rangle) \rangle}{\sigma^2}, \quad (7)$$

where $\langle \cdot \rangle$ denotes ensemble average and $\langle s \rangle$ is the estimated mean of the signal; for a time series with N points this is given by:

$$\langle s \rangle = \frac{1}{N} \sum_{n=1}^N s_n; \quad (8)$$

and the variance of the time series, σ^2 , can be estimated as:

$$\sigma^2 = \frac{1}{N-1} \sum_{n=1}^N (s_n - \langle s \rangle)^2 \quad (9)$$

A commonly used rule of thumb [15] for the calculation of sampling lag is to set V equal to the sampling lag required for the autocorrelation function to become negative. The problem with this approach is that it is only based on linear statistics, and it does not account for any nonlinear dynamical correlation.

3.2 Time Delay Calculation: Mutual Information Method

The other method for determining sampling delay is based on the mutual information function [5]. The original concept of mutual information was introduced in Shannon's

information theory, which gives a measure of the general independence of two variables. In our context, this function quantifies the information we have about the signal s_{n+V} given that we know s_n .

For a computational definition of this function, a histogram for the probability distribution of the signal is created. The probability that the signal has a value inside the i th bin of the histogram is denoted by p_i , and the probability that s_n is in bin i and s_{n+V} is in bin j is denoted by p_{ij} . Then the mutual information for sampling delay V can be defined as:

$$I(V) = \sum_{i,j} p_{ij}(V) \ln p_{ij}(V) - 2 \sum_i p_i \ln p_i \quad (10)$$

It should be noted that the value of mutual information is independent of the choice of histogram, as long as it is fine enough. For large values of V , s_n and s_{n+V} have no correlation with each other; $p_{ij} = p_i p_j$ and the mutual information becomes zero.

The sampling lag related to the first minimum of the mutual information function specifies the point where the information about s_{n+V} given knowledge of s_n or the redundancy has a local minimum. In general, the sampling lag value based on the autocorrelation function is not the same as the value from the mutual information function local minimum; however, it is often close. In such cases, it is better to select an optimal V inside that interval. Optimal values of V can then be verified through the visualization of the data in a two-dimensional embedding.

3.3 Calculation of Optimal Sampling Delay for Helicopter Flight Data

The autocorrelation function of our time series data is shown in Figure 7. It should be noted that this function is positive for small V , then becomes negative as V increases, then positive, etc., due to the quasi-periodic nature of s_n ; only the first interval of positive autocorrelation is shown. According to one criterion [15], the optimal value of sampling delay is near the point where the autocorrelation function has its first zero crossing; based on this figure it is between $V = 14$ and $V = 15$. For the final selection of the sampling delay, this result will be compared with that obtained from the mutual information function, and the final selection will be verified by visualizing the embedded data in the two-dimensional delay coordinates.

The mutual information function for the helicopter flight data is depicted in Figure 8. This function has a flat minimum around $V = 14$ to $V = 17$. Any value in this range should be a good choice for the sampling delay based on this criterion [5]. Again, the final optimal sampling delay will be selected after inspecting the helicopter flight data in two-dimensional delay coordinates.

Two-dimensional delay coordinate plots of the helicopter flight time-series data are portrayed in Figure 9 for six different values of sampling delay. As shown in this

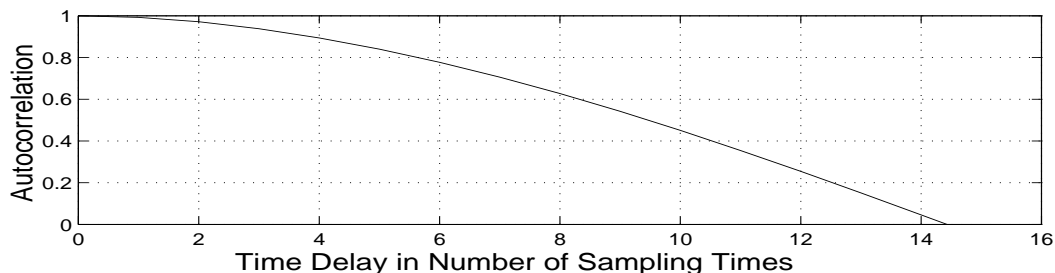


Figure 7: Autocorrelation function for the helicopter flight data

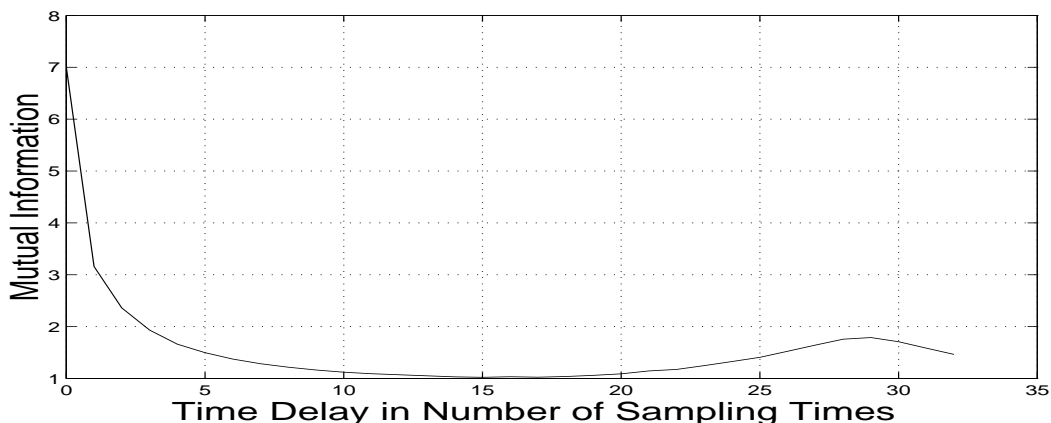


Figure 8: Mutual information function for the helicopter flight data

figure, for $V = 1$ the points are projected along the positive diagonal, indicating a high degree of correlation. Increasing the value of V up to the range suggested by the autocorrelation and mutual information approaches, we obtain better “unfolded” projections in the two-dimensional coordinates; increasing V beyond that range, all the points are projected near the negative diagonal, due to the negative autocorrelation for $V \cong 30$ due to quasiperiodicity. From this visualization, the optimal value of $V = 15$ is confirmed. It should be noted that other near-by values such as $V = 14$ and $V = 16$ also provide good projections.

3.4 Calculation of Optimal Sampling Delay for the Lorenz System

The mutual information plot for the variable $x(t)$ from the Lorenz System is shown in Figure 10. The first minimum of this function is around $V = 4$. This function is almost flat for higher values of V . The projection of the time series data of the Lorenz System in a 2-dimensional embedding space for $V = 1$ to $V = 8$ is presented in Figure 11. From the visualization provided in these plots, the optimal sampling

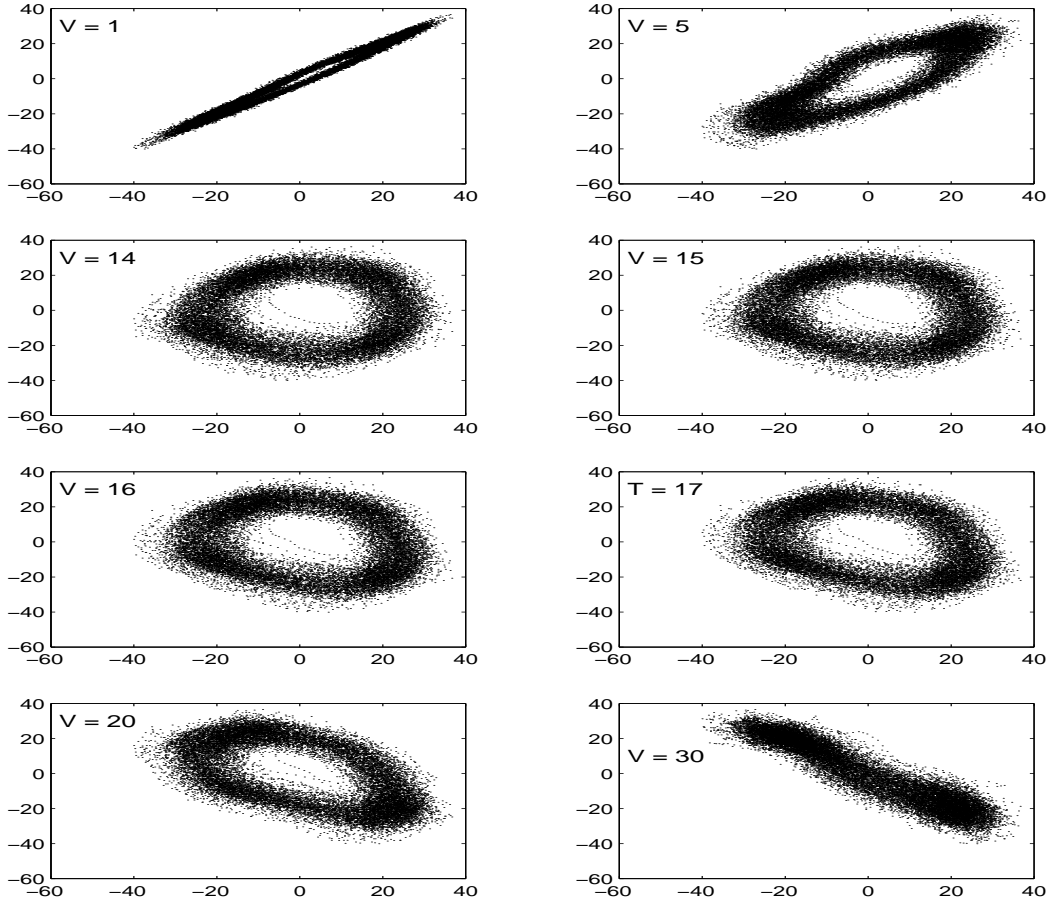


Figure 9: The two-dimensional embedding of flight data for different sampling delays

delay of $V = 4$ was chosen to obtain an optimal unfolding.

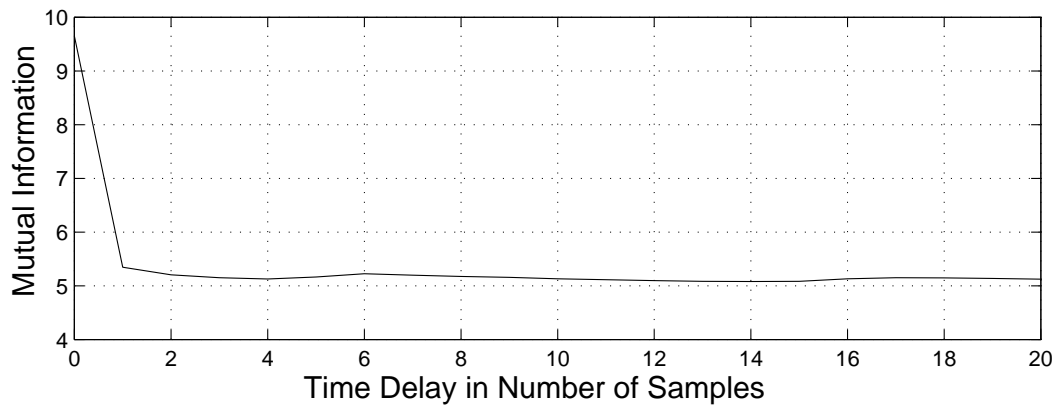


Figure 10: The mutual information function of $x(t)$ in the Lorenz System

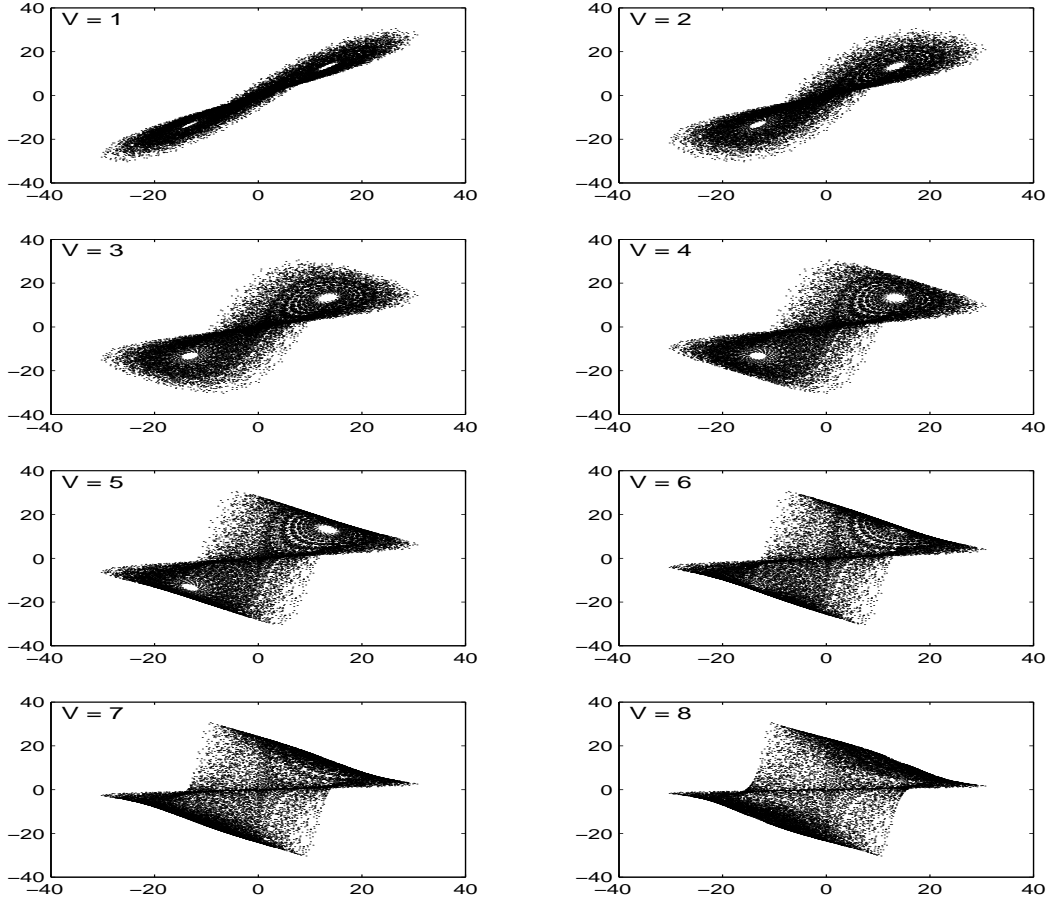


Figure 11: The two-dimensional embedding of $x(t)$ in the Lorenz System for different sampling delays

4 Reconstructed State Space Embedding Dimension

As discussed in Section 2, the other important parameter for state-space reconstruction is the embedding dimension. The embedding dimension, d , is the lowest integer dimension which unfolds the attractor in the projected space with no overlaps. Based on the embedding theorem [21], if the dimension of the attractor defined by the orbits in the original space is m , then the attractor can always be unfolded in an integer dimensional space of dimension d where $d > 2m$. This condition is the sufficient dimension for embedding; in most cases a lower dimension can unfold the attractor. In other words, it can be guaranteed that a delay-coordinate embedding with dimension higher than $2m + 1$ is never necessary. The most common approach for the calculation of embedding dimension, d , is the *false nearest neighbours* approach [9], which is explained below.

4.1 Embedding Dimension: False Nearest Neighbors Method

For a d -dimensional delay-coordinate reconstruction of s_n (for $n = 1, 2, \dots, N$), the delay vector at point k , $\mathbf{y}(k)$, can be written as:

$$\mathbf{y}(k) = [s_k, s_{k-V}, \dots, s_{k-(d-2)V}, s_{k-(d-1)V}], \quad k \geq (d-1)V + 1, \quad (11)$$

where V is found by the approach described in Section 3. The nearest neighbour of the vector $\mathbf{y}(k)$ is then determined, denoted by $\mathbf{y}^{NN}(k)$. In general, the vector $\mathbf{y}^{NN}(k)$ may be a true neighbour of $\mathbf{y}(k)$ due to its temporal nature, or it might be a false neighbour of $\mathbf{y}(k)$ due to projection from a higher dimension. In the former case, $\mathbf{y}^{NN}(k)$ is either the vector just behind or ahead of $\mathbf{y}(k)$ along its orbit. If the vector $\mathbf{y}^{NN}(k)$ is a false neighbour, the dimension d does not unfold the attractor, and going to a higher dimensions may move this false neighbour out of the neighbourhood of $\mathbf{y}(k)$. This procedure can be repeated for all the $\mathbf{y}(k)$ delay vectors, for $k = 1, 2, \dots, N$. During this approach, the value of d is increased incrementally until no more false neighbours are removed. At this point d is equal to the embedding dimension of d , and the attractor is completely unfolded [9].

In order to identify true and false neighbours, we use the Euclidean distance between the nearest neighbours in dimension d and $d+1$. In going to dimension $d+1$, the vectors $\mathbf{y}(k)$ and $\mathbf{y}^{NN}(k)$ are each augmented by s_{k-dV} and s_{k-dV}^{NN} , respectively. The Euclidean distance between the nearest neighbours in dimension d , denoted D_d , and in dimension $d+1$, D_{d+1} , can be formulated as:

$$D_d^2(k) = \sum_{i=1}^d [s_{k-(i-1)V} - s_{k-(i-1)V}^{NN}]^2 \quad (12)$$

$$D_{d+1}^2(k) = \sum_{i=1}^{d+1} [s_{k-(i-1)V} - s_{k-(i-1)V}^{NN}]^2 = D_d^2(k) + [s_{k-dV} - s_{k-dV}^{NN}]^2 \quad (13)$$

In fact, it is only necessary to compare the additional distance $|s_{k-dV} - s_{k-dV}^{NN}|$ with $D_d(k)$, the Euclidean distance in dimension d . If the additional distance in comparison to the distance of nearest neighbours in dimension d is large, the neighbours are false; otherwise, the neighbours are true. The normalized distance difference between dimension d and $d+1$ with respect to the distance in dimension d , ΔD_d , can be written as:

$$\Delta D_d(k) = \frac{|s_{k-dV} - s_{k-dV}^{NN}|}{D_d(k)} \quad (14)$$

Whenever the value of the index ΔD_d is greater than some predefined threshold, the neighbours are declared to be false. The value of this threshold is very important in declaring false neighbours. In general, the threshold value depends on the application, especially the noise level and the number of data points. If all regions of the attractor are sampled adequately, the variation of false neighbours with the number of data points is very small.

The false nearest neighbours method is very effective as long as the time series data are not corrupted by noise. In fact, for clean time series data the number of false nearest neighbours drops to zero as d approaches the embedding dimension. By increasing the delay-coordinate dimension beyond that point, the false nearest neighbours stay equal to zero, since after the attractor is unfolded for d , it stays unfolded for any dimension greater than d ; this situation holds as long as the data are not seriously corrupted by noise.

In real-life applications, the time series data are always contaminated by noise, and in some cases the noise may dominate the signal. For high noise levels, the embedding dimension would increase until the noise is also unfolded; since the dimension of noise is very high the false nearest neighbours may never decrease to zero. In such cases, we can stop increasing the value of d when the false nearest neighbours value comes to its first minimum. If the noise level is not very high, it is also possible to put the threshold value of false nearest neighbours greater than the noise level [9].

4.2 Dimension Calculation of the Reconstructed State Space

The false nearest neighbours index was used to calculate the delay-coordinate dimension of the helicopter time series data. The result of this calculation is presented in Figure 12. As shown, the value of the false nearest neighbours index is very close to zero for $d = 6$. This value will be selected for the delay-coordinate state-space reconstruction of our flight data.

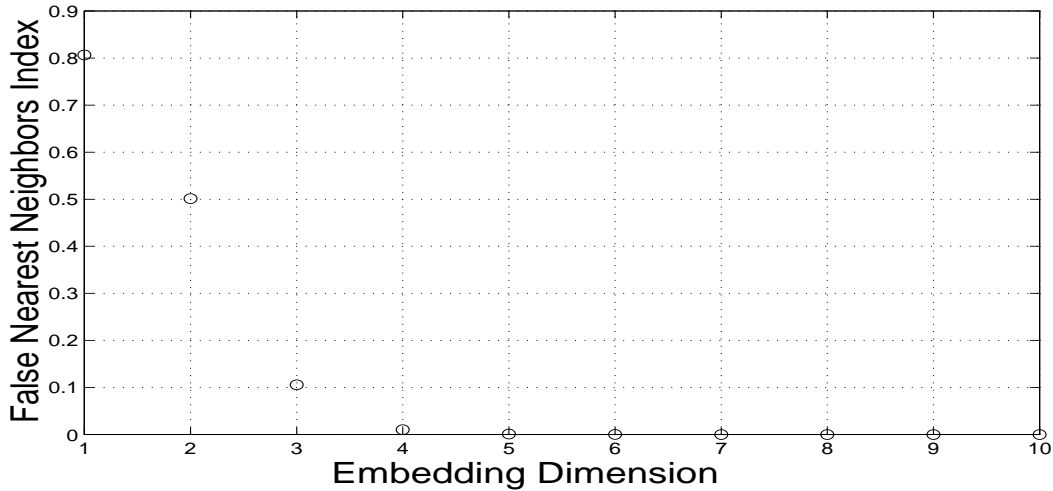


Figure 12: Calculation of embedding dimension by false nearest neighbours approach

4.3 Dimension Calculation of Reconstructed State Space for the Lorenz System

The delay-coordinate dimension of the Lorenz System was also calculated using the false nearest neighbours approach. Based on this, we found that a value of $d = 3$ can unfold the Lorenz System. This value is equal to the actual dimension of the system, $m = 3$. In the following analysis, the value of $d = 3$ is used as the minimum embedding dimension of the Lorenz System.

5 Lyapunov Exponents

In general, the trajectory of a dynamical system starting at an arbitrary initial point can end up at a stable fixed point (sink), a stable closed trajectory (periodic sink), a chaotic orbit, or it may become unstable. The evolution of such a trajectory may be quite complicated; for example, if an initial condition is near an unstable fixed point (source) p , it experiences an unstable behaviour in the beginning but at some distance from p , the orbit may be attracted to a sink q . Near the sink, the distance between the orbit points and the sink will decrease. This transient instability and attraction to a sink or period- K sink is not generic in all dynamical systems; in some systems, there may be no stable solutions or there may be chaotic orbits.

A chaotic orbit can be defined as continuously unstable but bounded behaviour of the system. Here the term “unstable” is not used to mean that the orbit completely diverges, as is the case for unstable fixed points or unstable closed trajectories (unstable limit cycles); rather, in such a system, given a point on a chaotic orbit there are points arbitrarily nearby on trajectories that will diverge from it during further evolution. This behaviour is in marked contrast to that of a stable limit cycle, where nearby points lead to converging trajectories. To discriminate between these phenomena (stable limit cycles and chaotic orbits), the maximal Lyapunov number (or maximal Lyapunov exponent) can provide a useful measure of the convergence or divergence (chaotic behaviour) of the system’s orbits. The maximal Lyapunov number is defined as the average per-step divergence rate of nearby points along a system’s orbits, and the maximal Lyapunov exponent is the natural logarithm of the maximal Lyapunov number.

5.1 Lyapunov Number/Exponent in One-Dimensional Maps

For simplicity, we discuss Lyapunov numbers and Lyapunov exponents in the context of maps; analogous developments for continuous-time systems should be evident. The stability of a discrete dynamical system around any fixed point is governed by the derivative of its map. For example, in a one-dimensional map \mathbf{F} with fixed point \mathbf{p} and

$\mathbf{F}'(\mathbf{p}) > 1$, the orbit of any point \mathbf{x} near \mathbf{p} will diverge from \mathbf{p} at a multiplicative rate of approximately $\mathbf{F}'(\mathbf{p})$ per iteration. Similarly, for a period- K orbit, the derivative of the K th iterate of the map determines the behaviour of the map. This derivative, according to the chain rule, is equal to the product of the map's derivatives at the K points of the orbit. In this case, the orbit of each point \mathbf{x} close to the periodic point \mathbf{p}_K , after each K iterations, converges to or diverges from \mathbf{p}_K at a rate about equal to the product of the derivatives.

The Lyapunov number is defined to quantify the average convergence or divergence of near-by points at each iteration. A Lyapunov number of 2 (or Lyapunov exponent of $\ln 2$) means that the average distance between the orbit of \mathbf{x}_1 and the orbit of a neighbouring point \mathbf{x}'_1 doubles each iteration. If the Lyapunov number is less than one (e.g. $\frac{1}{2}$), then the distance would be reduced (halved) at each iteration. For a period K orbit \mathbf{p}_K , we use the chain rule to formulate this measure as:

$$|(\mathbf{F}^K)'(\mathbf{p}_K)| = |\mathbf{F}'(\mathbf{x}_1)| |\mathbf{F}'(\mathbf{x}_2)| \dots |\mathbf{F}'(\mathbf{x}_K)| \quad (15)$$

To formalize this discussion, the sensitive dependence of chaotic systems on initial conditions can be distinguished from the behaviour of stable limit cycles (period- K sinks) by the Lyapunov number or exponent; clearly, these are the only two options given a vibratory signal that does not diverge in the traditional sense of instability. In fact, an orbit is chaotic if its Lyapunov number is greater than 1. In mathematical form, the Lyapunov number and exponent can be defined as follows:

Lyapunov number: Let \mathbf{F} be a one-dimensional map on \mathfrak{R} . The Lyapunov number, $L(\mathbf{x}_1)$, of the trajectory $\{\mathbf{x}_1, \mathbf{x}_2, \mathbf{x}_3, \dots\}$ is defined as:

$$L(\mathbf{x}_1) = \lim_{n \rightarrow \infty} (|\mathbf{F}'(\mathbf{x}_1)| |\mathbf{F}'(\mathbf{x}_2)| \dots |\mathbf{F}'(\mathbf{x}_n)|)^{1/n} \quad (16)$$

if this limit exists.

Lyapunov exponent: The Lyapunov exponent, $\lambda(\mathbf{x}_1)$, exists if and only if L exists, and can be defined as $\lambda(\mathbf{x}_1) = \ln L$

It should be noted that the Lyapunov number/exponent cannot be defined for any trajectory containing a point \mathbf{x}_i with $\mathbf{F}'(\mathbf{x}_i) = 0$. For a one-dimensional map \mathbf{F} , the Lyapunov number and exponent of a fixed point \mathbf{p} are:

$$L = |\mathbf{F}'(\mathbf{p})|, \quad \lambda = \ln |\mathbf{F}'(\mathbf{p})|, \quad (17)$$

and for a period- K point \mathbf{p}_K , the Lyapunov number and exponent are:

$$L(\mathbf{p}_K) = (|\mathbf{F}'(\mathbf{x}_1)| |\mathbf{F}'(\mathbf{x}_2)| \dots |\mathbf{F}'(\mathbf{x}_K)|)^{1/K}, \quad \lambda(\mathbf{p}_K) = \ln L(\mathbf{p}_K) \quad (18)$$

The unit of Lyapunov exponent is in inverse normalized time, and it provides a measure of the rate of divergence or convergence of nearby trajectories with each time step. In calculating the Lyapunov exponent, the time unit can be equal to the unit of the sampling time index or the unit of real time, say seconds [2].

5.2 Lyapunov Numbers and Exponents for Multidimensional Maps

Lyapunov numbers and exponents can also be defined for multidimensional maps. In a one-dimensional map, a single Lyapunov number gives a measure of separation rates of nearby points along the real line. For maps on \mathfrak{R}^m for $m > 1$, however, nearby points may diverge in one direction and converge in another. Therefore, in an m -dimensional map, each orbit has m Lyapunov numbers. These numbers measure the rate of expansion/contraction from the current point along m orthogonal directions. In general, the *maximal* Lyapunov number/exponent is the most important one for identifying chaotic behaviour of a system, since divergence (a positive Lyapunov exponent) in some direction(s) is a signature for chaos.

As an example, consider a 2-dimensional map with expansion on one direction and contraction on the other axis. Take a circle with unit radius centered on the first point \mathbf{x}_0 in the a state space. After each iteration of map \mathbf{F} on the points inside this disk, the points on the circle are expanded in one direction, and contracted in the other direction. This causes the unit circle to change into an ellipse. After each iteration of the mapping, the ellipse becomes longer and thinner. The result of this mapping for a unit circle after n iteration is shown in Figure 13. The expansion/contraction of the axes of the ellipse at each iteration is governed by the Lyapunov numbers. The natural logarithm of each Lyapunov number is the corresponding Lyapunov exponent.

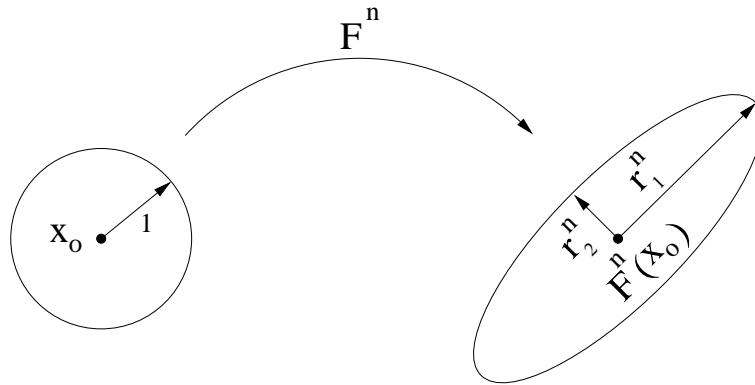


Figure 13: Effect of expansion and contraction in a 2-dimensional map [2]

In order to define the Lyapunov number in a multidimensional map, let the Jacobian (the first derivative matrix) of \mathbf{F} at \mathbf{x}_0 be denoted by $\mathbf{J}_0 = \mathbf{DF}(\mathbf{x}_0)$, and the Jacobian of the n th iterate of \mathbf{F} at \mathbf{x}_0 by $\mathbf{J}^n = \mathbf{DF}^n(\mathbf{x}_0)$. In the multidimensional case $m > 2$, the circle and ellipse are replaced by hypersphere and hyperellipsoid. Since we are considering the infinitesimal behaviour of map \mathbf{F} around \mathbf{x}_0 , the map can be approximated by its linearized model at \mathbf{x}_0 , $\mathbf{x}_{n+1} = \mathbf{J}_0\mathbf{x}_n$. Denoting the infinitesimal hypersphere of radius ϵ by U_ϵ , \mathbf{J}_0U_ϵ determines the hyperellipsoid with m orthogonal axes after the first iteration, and \mathbf{J}^nU_ϵ represents the hyperellipsoid after n iterations. The Lyapunov number can now be defined as follows:

Lyapunov number: Let \mathbf{F} be a smooth map on \mathfrak{R}^m , and for $k = 1, \dots, m$, let r_k^n be the length of the k th longest orthogonal axis of the hyperellipsoid $\mathbf{J}^n U_\epsilon$ divided by ϵ (the expansion/contraction) for an orbit with initial point \mathbf{x}_0 . Then r_k^n gives the expansion or contraction near the orbit at \mathbf{x}_0 during the first n iterations. The k th Lyapunov number at \mathbf{x}_0 is defined by:

$$L_k = \lim_{n \rightarrow \infty} (r_k^n)^{1/n}, \quad (19)$$

if the limit exists.

Lyapunov exponent: With similar notation, the k th Lyapunov exponent at \mathbf{x}_0 can be defined as $\lambda_k = \ln L_k$.

It should be noted that by definition, it is given that $L_1 \geq L_2 \geq \dots \geq L_m$ and $\lambda_1 \geq \lambda_2 \geq \dots \geq \lambda_m$.

According to the definitions above of Lyapunov number/exponent, a chaotic orbit in a multidimensional map can be defined as follows:

Chaotic orbit: Let \mathbf{F} be a map of \mathfrak{R}^m , $m \geq 1$, and let $\mathbf{x}_0, \mathbf{x}_1, \mathbf{x}_2, \dots$ be a bounded orbit of \mathbf{F} . The orbit is chaotic if:

1. it is not asymptotically periodic,
2. no Lyapunov number (exponent) is exactly one (zero), and
3. $L_1(\mathbf{x}_0) > 1$ ($\lambda_1(\mathbf{x}_0) > 0$).

In a chaotic system, the separation of nearby trajectories may be extremely fast. The average maximal rate of this divergence, characterized by the maximal Lyapunov exponent, characterizes the strength of the chaos. If the separation rate is averaged over a short time, we obtain a *local Lyapunov exponent*. Local Lyapunov exponents can have strong fluctuations [18], and are difficult to interpret. The (global) Lyapunov exponent is an average over the local values, and tends to be more consistent.

Again, the maximal Lyapunov exponent, λ_1 , is the most important. From the value of λ_1 for a particular trajectory, we can determine if the system has a stable fixed point, a stable limit cycle, or if it exhibits chaotic behaviour. Dissipative systems have a negative maximal Lyapunov exponent, and separate trajectories are attracted to a stable fixed point. These trajectories approach each other exponentially fast when they are approaching the stable fixed point. If the system has a stable limit cycle, two separate trajectories can approach each other exponentially ($\lambda_1 < 0$) or more slowly than exponentially ($\lambda_1 = 0$). In a chaotic system, the maximal Lyapunov exponent is positive, $\lambda_1 > 0$; in this case, the nearby trajectories diverge from each other exponentially fast. Note that for a random noise, the maximal Lyapunov exponent is infinite. A summary of system behaviour and its relation with the Lyapunov exponent is summarized in Table 1 [8].

Table 1: Relation of Maximal Lyapunov Exponent and System Behaviour

Type of motion	Maximal Lyapunov exponent
stable fixed point	$\lambda_1 < 0$
stable limit cycle	$\lambda_1 \leq 0$
chaos	$0 < \lambda_1 < \infty$
noise	$\lambda_1 = \infty$

It should be mentioned that the Lyapunov exponent is an *invariant* of the system. In numerical calculation of Lyapunov exponents from time series data, as long as the data has enough resolution, the type of measurement, sampling time, or use of a smooth transformation does not change the resulting values of the Lyapunov exponents. In calculating Lyapunov exponents using the delay-coordinate embedding approach, the local Lyapunov exponent varies throughout the attractor, and the actual exponent is an appropriate average over the whole space.

5.3 Determining the Maximal Lyapunov Exponent from Time Series Data

As mentioned, the maximal Lyapunov exponent is of paramount importance. For this reason, most algorithms used in the study of chaos deal with the calculation of this exponent. In this section, an algorithm which calculates the maximal Lyapunov exponent from time series data is discussed [7, 17]. In this algorithm, the exponential divergence of nearby trajectories is tested. Thus, for data with no finite exponent, such as noise, no Lyapunov exponent will be calculated.

Recall that the (global) Lyapunov exponent is an average over the local Lyapunov exponent in the whole attractor space. In another words, the Lyapunov exponent is the average of exponential expansion/contraction rates over the whole time series data. In most cases, the time series data are contaminated by noise. In order to reduce the effect of noise on the calculation of the Lyapunov exponent, some appropriate averaging (filtering) method may deployed if the noise level is substantial.

The Lyapunov exponent can be calculated using the delay-coordinate embedding approach as follows:

1. Set $l = 1$.
2. Select a reference point s_l from the time series data, $l > (d - 1)V$, and identify $\mathbf{y}(l)$ in the delay-coordinate embedding space as:

$$\mathbf{y}(l) = [s_l, s_{l-V}, \dots, s_{l-(d-2)V}, s_{l-(d-1)V}] \quad (20)$$

where the values of V and d are calculated as discussed in Sections 3 and 4, respectively.

3. Find all the points in the neighbourhood of $\mathbf{y}(l)$ with the distance smaller than ϵ , $U_\epsilon(\mathbf{y}(l))$.
4. Calculate $\bar{\delta}_l(0)$, the average of the distances between $\mathbf{y}(l)$ and the points in $U_\epsilon(\mathbf{y}(l))$.
5. Calculate $\bar{\delta}_l(\Delta k)$, the average of the same distances after Δk time steps, for $\Delta k = 1, 2, \dots$.
6. Set $l = l + 1$; return to Item 2 until sufficient points are tested, $l = 2, 3, \dots L$.
7. Calculate the logarithm of the averaged calculated values of Item 5 over all the data points, $D_L(\Delta k)$.
8. Plot the calculated values of Item 7, $D_L(\Delta k)$, versus Δk . The slope of this graph is the Lyapunov exponent per time step. This value can be converted to the normal time unit.

The selected value of ϵ should be as small as possible, but it should be large enough that each point has at least several neighbours. This causes all parts of the attractor to participate in the calculation, and thus a better value of the Lyapunov exponent is obtained.

In order to minimize computational effort, it is possible to reduce the number of data points used during the above calculations. One option is to stop the computation as soon as a sufficient number of reference points with rich neighbourhoods have been obtained. The minimum number of reference points can be as low as 500 points, and the number of neighbours for each reference point should be greater than 10 [8]. In general, reference points with fewer neighbours will cause more fluctuation in the value of D_L . Fluctuations in D_L can also occur due to the presence of noise in the data set. If the noise level is bigger than ϵ , some false neighbours may be considered as true neighbours, and the value of D_L will thereby be corrupted.

5.4 Calculation of the Maximal Lyapunov Exponent for Helicopter Flight Data

The helicopter flight data set is studied by using the method explained in Section 5.3. The sampling delay and embedding dimension were varied in different studies, and two methods were used, to rigorously confirm our results. The value of $D_L(\Delta k)$ is calculated by the methods described in [7] and [17]. The following results were obtained using software supplied by the authors [7, 17].

Study 1: Using the approach described in [7], the value of $D_L(\Delta k)$ is calculated for neighbourhood sizes of $\epsilon = 6$ and $\epsilon = 8$, and five different dimensions $d = 6, 7, \dots, 10$, resulting in 10 cases. The selected number of reference points is equal to $L = 1000$,

and the number of points in the ϵ -neighbourhood of reference points with the selected ϵ was from 50 to 1000. All the plots are presented in Figure 14.

In this figure, we note that a similar behaviour is obtained in each case. The initial strong fluctuation of D_L are due to the presence of quasiperiodicity in the dynamical system. Underlying these fluctuations, a distinct linear increase is apparent, as shown by the dashed line. The slope of this line gives the estimated value of the maximal Lyapunov exponent. The calculated value of maximal Lyapunov exponent from Figure 14 is $\lambda_1 = 3.0 * 10^{-3} \text{ (time step)}^{-1}$ or $\lambda_1 = 3.07 \text{ second}^{-1}$.

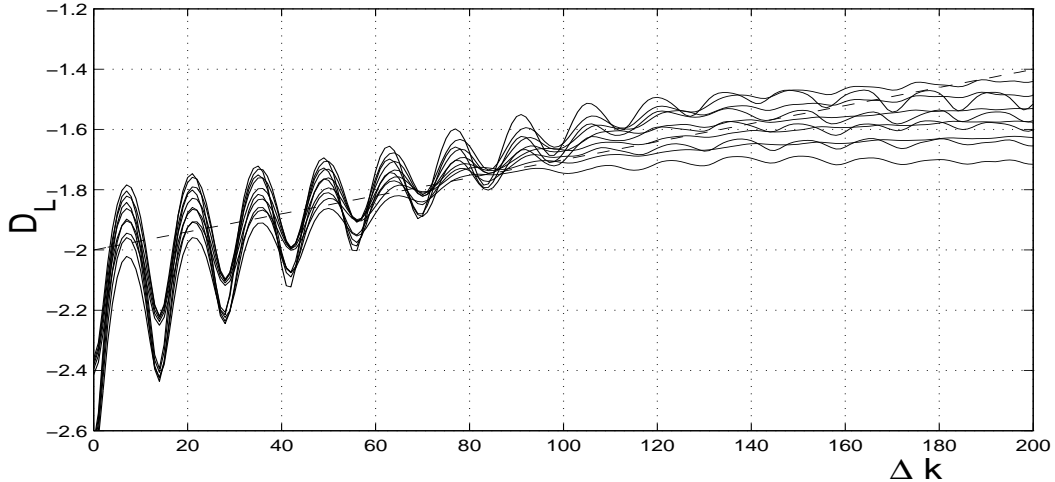


Figure 14: Maximal Lyapunov exponent calculation for helicopter flight data by the method of Kantz [7]

Study 2: The maximum Lyapunov exponent is also calculated by the approach mentioned in [17]. In this method, the value of ϵ is automatically changed until a sufficient number of neighbors are found; the dimension values of $d = 6, 10, 14, 18$ are examined. The plots obtained from this method are portrayed in Figure 15, with a dashed line with the same slope as shown in Figure 14. In this figure, the plot for $d = 6$ has the same linear increase as mentioned above, and the slope of the other plots will decrease when the value of d increases. This decrease could be due to corruption of the data with noise. As mentioned in [8], noise can have a major impact on the computation of the maximal Lyapunov exponent. To calculate the maximal Lyapunov exponent more accurately, the measured data should be filtered very precisely. Many linear and nonlinear filtering algorithms for chaotic data are proposed in the literature; we have not pursued this, due to the low level of noise evident in Figure 2.

Study 3: To investigate the effect of sampling delay on the computed maximal Lyapunov exponent, we chose the dimension $d = 6$ and several values of sampling delay, $V = 10, 11, 12, 14, 16$ and 18 . The results for these cases by the method of [17] are shown in Figure 16. In all the plots, the dashed line has a slope equal to the above-mentioned value. As it is clear from these plots, changing V slightly

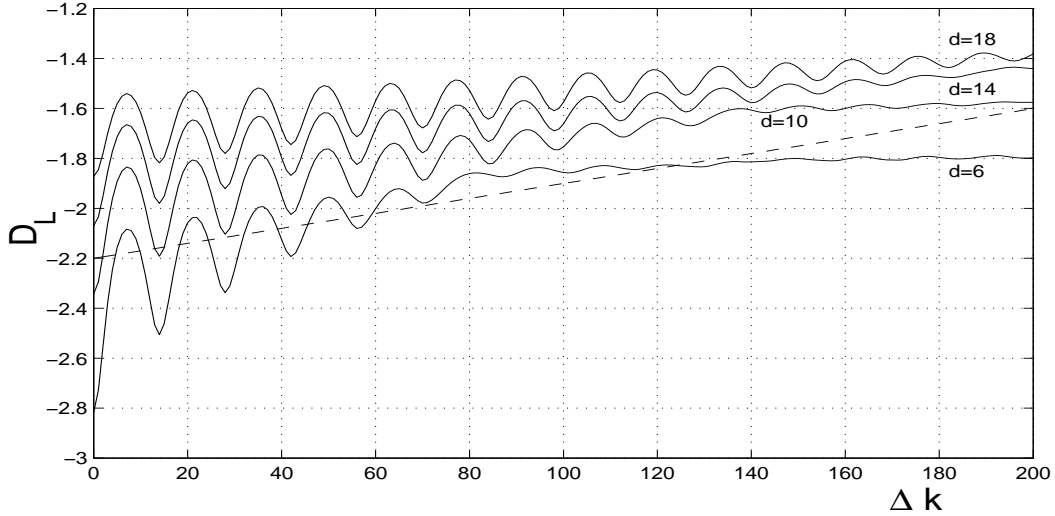


Figure 15: Maximal Lyapunov exponent calculation for the helicopter flight by the method of Rosenstein *et al* [17]

($12 \leq V \leq 16$) does not have much impact on λ_1 , but larger and smaller values can have some effect on the computed value of λ_1 .

Study 4: It should be noted that in real-life time series, the number of data points and sampling time can also have some effect on the computed Lyapunov exponent. To study this, a new data set FDS'_1 is created by removing every other point of the original data FDS_1 . Using the same approaches, the new optimal sampling delay, V , and embedding dimension are estimated. Plots for the new data set for $V = 7$ and four different values of dimension, $d = 6, 10, 14,$ and 18 from the approach of [17] are presented in Figure 17. The dashed line has the slope of $\lambda_1 = 5.98E - 3$ (time step) $^{-1}$ or 3.06 second^{-1} . Comparing this result with that of Study 1, it can be concluded that the sampling time has only a slight effect on the calculated value of λ_1 .

5.5 Calculation of the Maximal Lyapunov Exponent for the Hénon Map and Lorenz System

In order to confirm our computation of λ_1 , two classical problems are also examined. As an example of a discrete system, the value of λ_1 for the Hénon Map by the approach of Kantz [7] is calculated. The plots of D_L for this map for $d = 2, 3, 4,$ and several values of ϵ is shown in Figure 18. The value of λ_1 as reported in the literature is 0.418 [17]. The slope of the dashed line in Figure 18 is 0.418 ; as can be seen, the slopes of the D_L plots are very close to the slope of the dashed line.

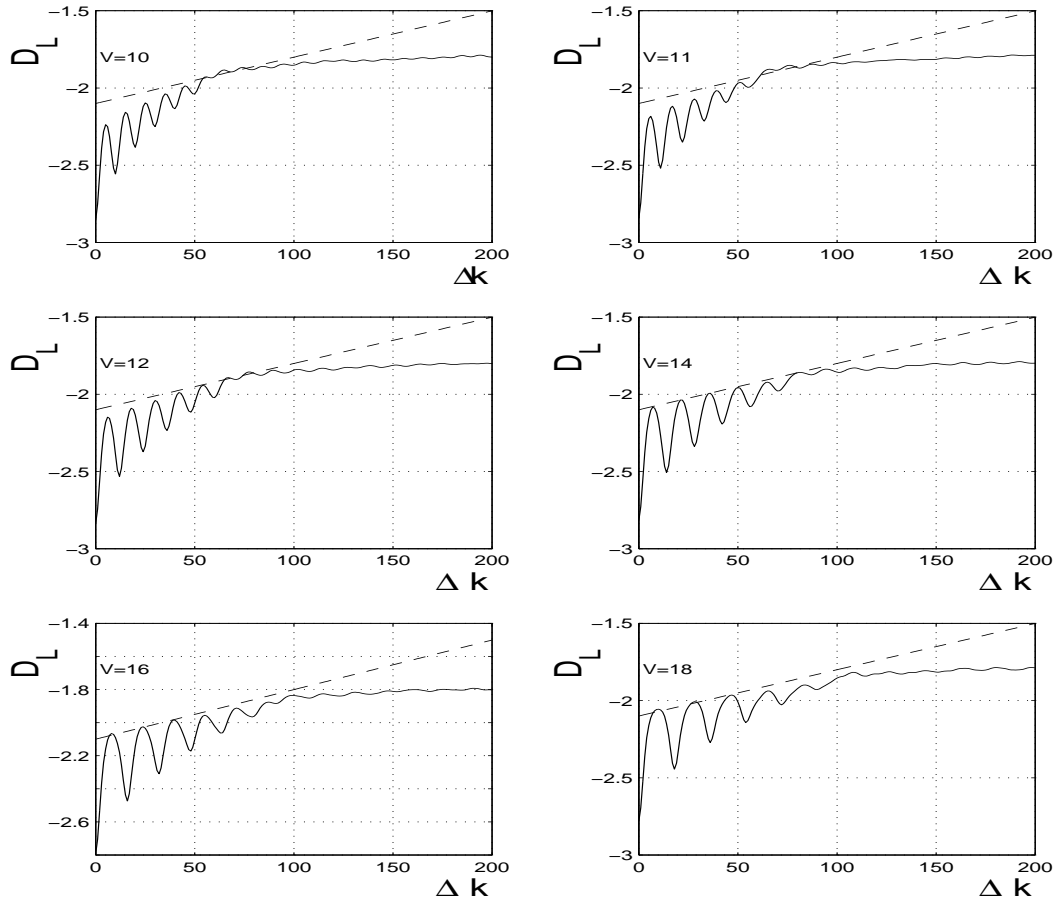


Figure 16: The effect of reconstruction sampling delay on maximal Lyapunov exponent computation for $d = 6$

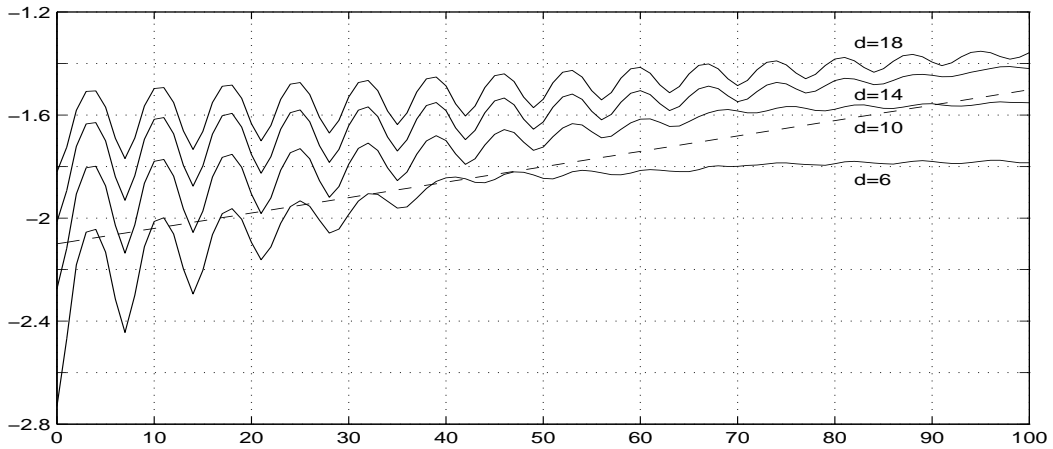


Figure 17: Maximal Lyapunov exponent computation for data set FDS'_1 by the method of Rosenstein *et al* [17]

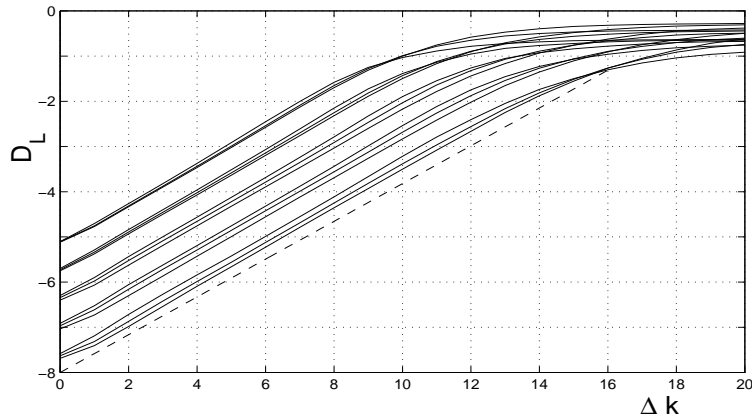


Figure 18: Maximal Lyapunov exponent calculation for the Hénon Map by the approach of Kantz [7]

The maximal Lyapunov exponent of $x(t)$ for the Lorenz System is also computed using the approach of Kantz [7]. The value of D_L is calculated for $d = 3, 4, 5, 6$, and several values of ϵ ; the corresponding plots are depicted in Figure 19. The dashed lines in Figure 19 have a slope equal to the accepted value of $\lambda_1 = 1.5$ [17], so it is clear that the slope of D_L is in accordance with the reported value in the literature. The fluctuation of D_L in this figure is related to the use of small values of ϵ .

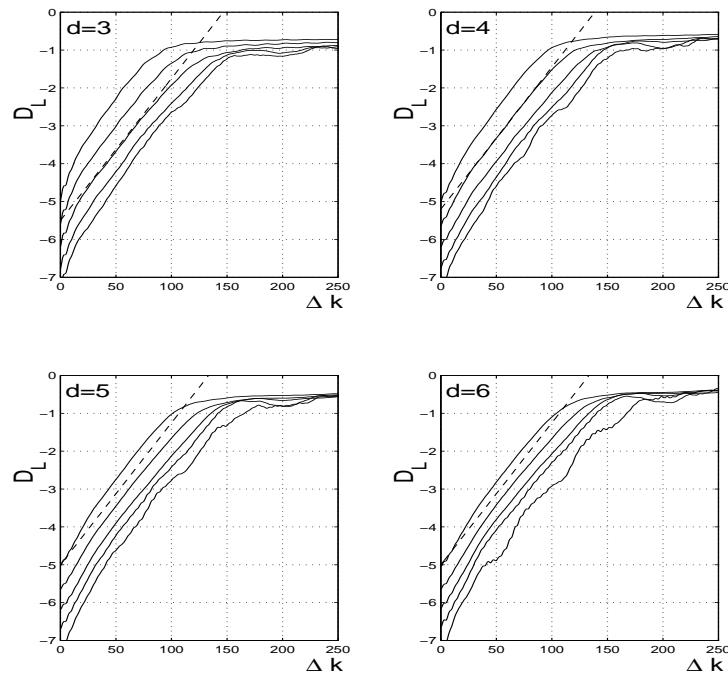


Figure 19: Maximal Lyapunov exponent calculation of $x(t)$ in the Lorenz System by the approach of Kantz [7]

6 Conclusion

A detailed analysis of helicopter flight data has been performed in order to investigate the possibility of chaotic behaviour. The motivation of this study was to determine the vibrational characteristics of a helicopter during flight. Two sets of flight data related to the acceleration of the helicopter for different airspeeds were considered. The data were sampled at $f_s=1024$ Hz at the nominal rotor speed of $f_n = 3.57$ Hz, when the active vibration control of helicopter is switched off.

As a first step, the time series data was inspected in the frequency domain. The blade passing frequency of $f_{BP}=17.85$ Hz has the highest amplitude in the power spectrum of the data (Figure 3); however, significant power over a broad range of frequencies is also present. The general sources of broad band frequency content can be random noise or chaos. The data sequences provided do not appear to be noisy; for this reason, the presence of chaos in the time series data may be suspected.

One of the major characteristics of chaotic systems is their sensitive dependence of their trajectory to the initial conditions. Two trajectories with very close initial conditions can diverge rapidly as time passes. This characteristic can be quantified by the Lyapunov exponent; in particular, chaotic systems have a maximal Lyapunov exponent greater than zero. In order to calculate the maximal Lyapunov exponent, the given time series data were used to reconstruct a state-space representation. The delay-coordinate embedding approach was used for this purpose.

The selection of sampling delay and dimension of the embedding space were the main considerations. The optimal sampling delay for the helicopter time series data was determined using the autocorrelation and mutual information functions. The final selection was verified by inspecting the data embedded in a 2-dimensional delay-coordinate state space. The dimension of the helicopter data was computed by the false nearest neighbours approach.

The maximal Lyapunov exponent of the embedded system was calculated by two of the methods proposed in the literature and using software supplied by the authors. The maximum Lyapunov exponent derived from the helicopter data was equal to $\lambda_1 = 3.0 * 10^{-3} (\text{time step})^{-1}$ or $\lambda_1 = 3.07 \text{ second}^{-1}$. This value is greater than zero, and shows the exponential divergence of nearby points. As a result, the system appears to have a chaotic behaviour.

7 References

- [1] H. D. I. Abarbanel, *Analysis of Observed Chaotic Data*, Springer, 1996.
- [2] K. T. Alligood, T. D. Sauer, J. A. Yorke, *An Introduction to Dynamical Systems*, New York: Springer-Verlag, 1997.

- [3] Casdagli, M., “Chaos and deterministic versus stochastic nonlinear modeling” *Journal of the Royal Statistical Society B*, 54, 1991.
- [4] Casdagli, M. , Eubank, S., Farmer, J. D., Gibson, J. “State space reconstruction in the presence of noise” *Physica D*, 51, 1991.
- [5] A. M. Fraser, H. L. Swinney, “Independent coordinates for strange attractors from mutual information” , *Physical Review A*, 33, 1986.
- [6] S. Hayes, C. Grebogi, E. Ott, “Communicating with chaos” *Physical Review Letters*, 70, 1993.
- [7] H. Kantz “A robust method to estimate the maximal Lyapunov exponent of a time series”, *Physical Review A*, 185, 1994.
- [8] *Nonlinear time series analysis*, by Holger Kantz, Maz Planck Institute for Physics of Complex Systems, Dresden Thomas Schreiber, Physics Department, University of Wuppertal, 1997.
- [9] M. B. Kennel, R. Brown, and H. D. I. Abarbanel, “Determining embedding dimension for phase-space reconstruction using a geometrical construction” , *Physical Review A*, 45, 1992.
- [10] D. Kugiumtzis, B. Lillekjendlie, N. Christophersen, “Chaotic time series I” , *Modeling, Identification and Control*, 15, 1994.
- [11] W. Liebert, H. Schuster, “Proper choice of the time delay for the analysis of chaotic time series” *Physical Review A*, 142, 1989.
- [12] A. I. Mees, P. E. Rapp, L. S. Jennings, “ Singular-value decomposition and embedding dimension” , *Physical Review A*, 36, 1987.
- [13] E. Ott , C. Grebogi, J. A. Yorke, “Controlling chaos, controlling chaotic dynamical systems” *Physical Review Letters*, 64, 1996; also in CHAOS/XAOC, American Physical Society, edited by D. Campbell, 1990, pp. 77-80.
- [14] E. Ott, *Chaos in Dynamical Systems*, Cambridge University Press, 1993.
- [15] E. Ott, T. Sauer, J. A. Yorke, *Coping with Chaos: Analysis of Chaotic Data and the Exploitation of Chaotic systems*, New York, Wiley, 1994.
- [16] N. Packard, J. Crutchfield, J. D. Farmer, R. Shaw, “Geometry from a time series” , *Physical Review Letters*, 45 (9), 1980.
- [17] M. T. Rosenstein, J. J. Collins, C. J. De Luca, “A practical method for calculating largest Lyapunov exponents from small data sets” , *Physica D*, 65, 1993.
- [18] M. Sano and Y. Sawada, “Measurement of the Lyapunov spectrum from a chaotic time series” , *Physical Review Letters*, 55, 1985.

- [19] T. Sauer, J. Yorke, and M. Casdagli, “Embedology”, *Journal of Statistical Physics*, 65, 1991.
- [20] Johan A. K. Suykens, and Joos Vandewalle, Eds., *Nonlinear Modeling: Advanced Black-Box Techniques*, Springer, 1998.
- [21] F. Takens, “Detecting strange attractors in turbulence”, in *Dynamical Systems and Turbulence*, Edited by D. A. Rand and L.-S. Young, Warwick 1980.